Articles

Catalytic Cycling in β-Phosphoglucomutase: A Kinetic and Structural Analysis[†,‡]

Guofeng Zhang, Jianying Dai, Liangbing Wang, and Debra Dunaway-Mariano*

Department of Chemistry, University of New Mexico, Albuquerque, New Mexico 87131-0001

Lee W. Tremblay and Karen N. Allen*

Department of Physiology and Biophysics, Boston University School of Medicine, Boston, Massachusetts 02118-2394

Received March 26, 2005; Revised Manuscript Received May 18, 2005

ABSTRACT: *Lactococcus lactis* β-phosphoglucomutase (β-PGM) catalyzes the interconversion of β-D-glucose 1-phosphate (β-G1P) and β-D-glucose 6-phosphate (G6P), forming β-D-glucose 1,6-(bis)phosphate (β-G16P) as an intermediate. β-PGM conserves the core domain catalytic scaffold of the phosphatase branch of the HAD (haloalkanoic acid dehalogenase) enzyme superfamily, yet it has evolved to function as a mutase rather than as a phosphatase. This work was carried out to identify the structural basis underlying this diversification of function. In this paper, we examine β-PGM activation by the Mg^{2+} cofactor, β-PGM activation by Asp8 phosphorylation, and the role of cap domain closure in substrate discrimination. First, the 1.90 Å resolution X-ray crystal structure of the Mg^{2+}−β-PGM complex is examined in the context of previously reported structures of the Mg^{2+}−α-D-galactose-1-phosphate−β-PGM, Mg^{2+}−phospho-β-PGM, and Mg^{2+}−β-glucose-6-phosphate-1-phosphorane−β-PGM complexes to identify conformational changes that occur during catalytic turnover. The essential role of Asp8 in nucleophilic catalysis was confirmed by demonstrating that the D8A and D8E mutants are devoid of catalytic activity. Comparison of the ligands to Mg^{2+} in the different complexes shows that a single Mg^{2+} coordination site must alternatively accommodate water, phosphate, and the phosphorane intermediate during catalytic turnover. Limited involvement of the HAD family metal-binding loop in Mg^{2+} anchoring in β-PGM is consistent with the relatively loose binding indicated by the large K_m for Mg^{2+} activation (270 ± 20 μM) and with the retention of activity found in the E169A/D170A double loop mutant. Comparison of the relative positions of cap and core domains in the different complexes indicated that interaction of cap domain Arg49 with the "nontransferring" phosphoryl group of the substrate ligand might stabilize the cap-closed conformation, as required for active site desolvation and alignment of Asp10 for acid−base catalysis. Kinetic analyses of the specificity of β-PGM toward phosphoryl group donors and the specificity of phospho-β-PGM toward phosphoryl group acceptors were carried out. The results support a substrate induced-fit mechanism of β-PGM catalysis, which allows phosphomutase activity to dominate over the intrinsic phosphatase activity. Last, we present evidence that the autophosphorylation of β-PGM by the substrate β-G1P accounts for the origin of phospho-β-PGM in the cell.

Phosphoglucomutases catalyze the interconversion of D-glucose 1-phosphate (G1P) and D-glucose 6-phosphate (G6P).[1] Operating in the forward G6P-forming direction, this reaction links polysaccharide phosphorolysis to glycolysis. In the reverse direction, the reaction provides G1P for the biosynthesis of exo-polysaccharides (*8*). There are two classes of phosphoglucomutases, the α-phosphoglucomutases (α-PGM, EC 5.4.2.2), ubiquitous among eukaryotes and prokaryotes, and the β-phosphoglucomutases (β-PGM, EC 5.4.2.6), present in certain bacteria and protists. The two classes of mutases are distinguished by their specificity for α- and β-D-glucose phosphates and by their protein fold

[†] This work was supported by NIH Grant GM61099 (to D.D.-M. and K.N.A.).

[‡] The X-ray coordinates are listed in the Protein Data Bank as entry 1ZOL.

* To whom correspondence should be addressed. D.D.-M.: telephone, (505) 277-3383; fax (505) 277-6202; e-mail, dd39@unm.edu. K.N.A.: telephone, (617) 638-4398; fax, (617) 638-4285; e-mail, allen@med-xtal.bu.edu.

[1] Abbreviations: α-PGM, α-phosphoglucomutase; α-PGM/PMM, dual-specificity α-phosphoglucomutase/α-phosphomannomutase; β-PGM, β-phosphoglucomutase; E, β-PGM−Mg^{2+}; E−P, phospho-β-PGM−Mg^{2+}; E−P−GP, β-PGM−β-glucose-6-phosphate-1-phosphorane−Mg^{2+}; β-G1P, β-D-glucose 1-phosphate; β-G16P, β-D-glucose 1,6-(bis)phosphate; α-G1P, α-D-glucose 1-phosphate; α-G16P, α-D-glucose 1,6-(bis)phosphate; α-F16P, α-D-fructose 1,6-(bis)phosphate; pNPP, *p*-nitrophenyl phosphate; G6P, α- and/or β-D-glucose 6-phosphate; NADP, adenine dinucleotide 3′-phosphate; K^+Hepes, potassium salt of 4-(2-hydroxyethyl)-1-piperazineethanesulfonic acid; K^+Ches, potassium salt of *N*-cyclohexyl-2-aminoethanesulfonic acid; K^+Mes, potassium salt of 2-(*N*-morpholino)ethanesulfonic acid; DTT, dithiothreitol; EDTA, ethylenediaminetetraacetic acid; HPLC, high-performance liquid chromatography; SDS−PAGE, sodium dodecyl sulfate−polyacrylamide gel electrophoresis; SA, specific radioactivity; MLF, maximum likelihood target using amplitudes.

10.1021/bi050558p CCC: $30.25
Published on Web 06/17/2005

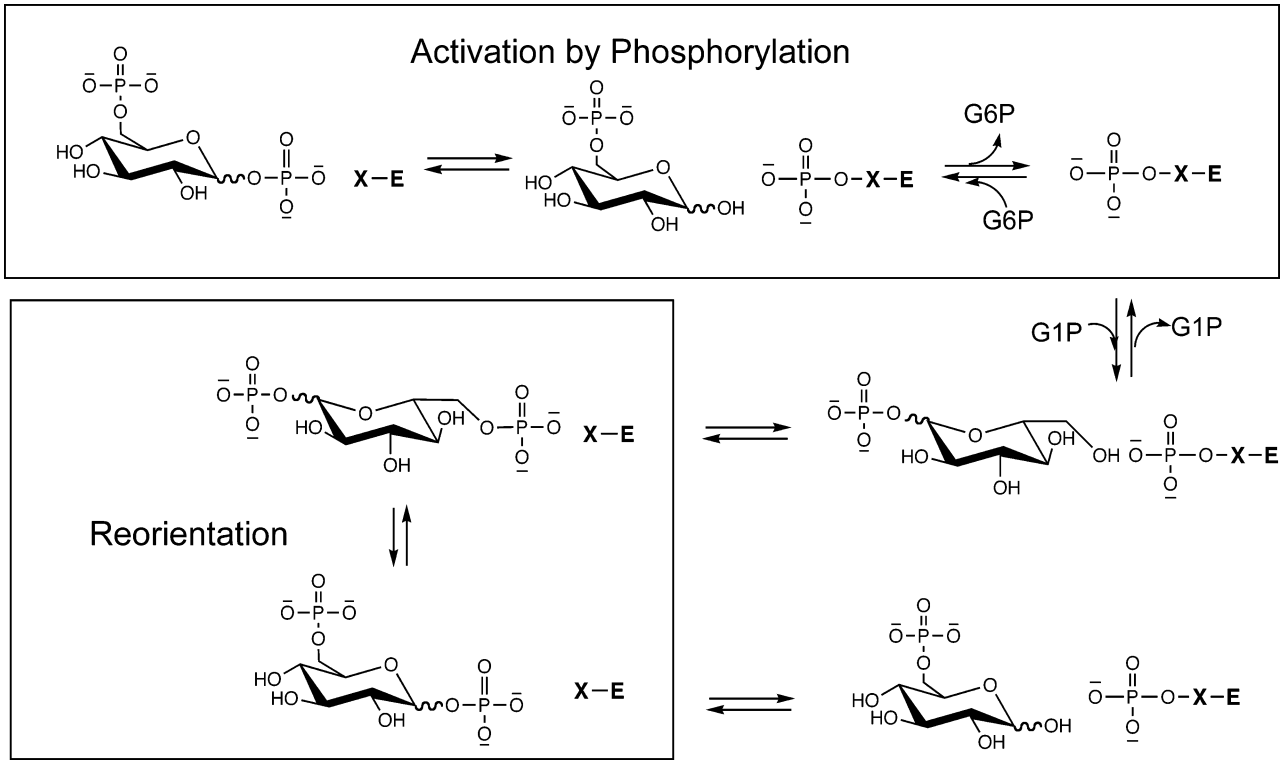

FIGURE 1: Sequence of reaction steps involved in a single catalytic cycle in enzymes α-PGM and β-PGM. For α-PGM, the substrate is αG1P, the intermediate is α-G16P, and the active site nucleophile (X) is Ser108. For β-PGM, the substrate is β-G1P, the intermediate is β-G16P, and the active site nucleophile (X) is Asp8.

family. α-PGM belongs to the phosphohexomutase superfamily (*9*), while β-PGM belongs to the haloalkanoic acid (HAD) enzyme superfamily (*10*). The four-domain α-PGMs (∼50 kDa) (*11*−*14*) are approximately twice the size of the two-domain β-PGMs (∼25 kDa) (*15*). The common denominator between the mutases is catalysis via a glucose 1,6-(bis)phosphate (G16P) intermediate. Whereas α-PGM catalysis had been studied in depth (*16*−*31*), comparatively little is known about β-PGM catalysis, the topic of this paper.

The catalytic cycles of two divergent α-PGMs, one from rabbit muscle (*11*, *12*, *28*−*30*) that functions in energy metabolism and the other from *Pseudomonas aeruginosa* [the duel specificity α-phosphoglucomutase/α-phosphomannomutase (α-PGM/PMM)] (*13*, *14*, *32*, *33*) that functions in alginate and lipopolysaccharide biosynthesis (*34*−*36*), have been shown to be the same. The cycle consists of phosphorylation of α-G1P by a phosphorylated active site serine residue to form α-G16P as an intermediate, reorientation of the intermediate in the active site, transfer of the C(1) phosphoryl group to the active site serine, and finally release of G6P from the active site of the phosphorylated enzyme (*25*, *33*) (Figure 1). Phosphorylated α-PGM is chemically stable in water (half-life of ∼7 years) yet transfers its phosphoryl group to α-G1P at a rate of 1000 s^{-1} (*37*). It has been presumed that in vivo α-PGM is phosphorylated by α-G16P [K_m for activation = 0.1 μM for *P. aeruginosa* α-PGM/PMM (*32*); K_d = 0.02 μM for rabbit muscle α-PGM (*37*, *38*)], even though the source of α-G16P in the cell has not yet been established. An alternate proposal is that α-PGM is autophosphorylated by ATP, an activity that has been observed in vitro (*22*).

β-PGM isolated from *Lactococcus lactis* (*39*), *Bacillus subtilis* (*40*), *Neisseria perflava* (*41*), and *Euglena gracilis* (*42*) is, like α-PGM, known to utilize G16P as a phosphoryl donor and Mg^{2+} as a cofactor. However, there are distinct differences between the two catalytic scaffolds, which suggests that the respective phosphoenzymes are generated and stabilized by different mechanisms. X-ray crystallographic analysis of *L. lactis* β-PGM has provided three snapshots of the enzyme bound with its cofactor (Mg^{2+}) and a phosphorylated ligand (*43*, *44*, *58*). These structures differ in the identity of the ligand and the solvent accessibility of the active site. The initial structure pictured the phosphoenzyme in an active site open conformation; the second structure showed the enzyme in an active site closed conformation with the Asp8 carboxylate oxygen forming a covalent bond to the phosphorus of the β-glucose-6-phosphate-1-phosphorane, and the third structure revealed the enzyme in an active site closed conformation, with the substrate analogue α-D-galactose 1-phosphate oriented to place its phosphate group at the distal phosphate binding site and its C(6)OH group near the Asp8 nucleophile. The first two structures represent reaction intermediates stabilized in the crystalline state and the third an inhibitory, dead-end complex of substrate bound to the dephosphoenzyme. In this paper, we report the structure of a fourth complex, the "free" holoenzyme bound to its Mg^{2+} cofactor. Within the catalytic cycle, this enzyme form binds and is phosphorylated by G16P. Herein, the four structures are compared, and kinetic studies probing structural requirements for β-PGM phosphorylation and dephosphorylation are reported, to provide insight into how the phosphatase branch of the HAD family (*45*) has acquired phosphomutase function, and how the β-PGM catalytic strategy differs from that used by α-PGM.

MATERIALS AND METHODS

Enzymes and Reagents

L. lactis β-PGM (Swiss-Prot entry P71447) and sugar phosphate phosphatase BT4131 from the bacterium *Bacteroides thetaiotaomicron* VPI-5482 were prepared from the *Escherichia coli* clones as previously described (*15*, *46*). D-[1-^{14}C]Glucose 6-phosphate (SA = 49.3 mCi/mmol) was purchased from Perkin-Elmer Life Sciences. Kinetic assay and protein purification materials were purchased from Sigma-Aldrich. The Malachite Green-based (*47*, *48*) phosphate assay kit was purchased from BioMol Co. and used in phosphate determinations of the PEG 4000 (Hampton Research) and PEG 3350 (Fluka). Protein concentrations were determined using the Bradford method (*49*). Radioactivity was measured using Ultima Gold liquid scintillation cocktail (Perkin-Elmer) and a Beckman LS 6500 multipurpose scintillation counter.

Crystallization and Structure Determination

Crystallization conditions for the β-PGM$-$Mg^{2+} complex were obtained by sparse-matrix screening (*50*) with Crystal Screen Kits I and II (Hampton Research). For crystallization, the purified recombinant *L. lactis* β-PGM ($\sim$25 mg/mL) was dissolved in 1 mM Hepes (pH 7.3) and 10 mM $MgCl_2$. Crystals grew at 18 °C as rectangular plates with overall dimensions of approximately 1 mm $\times$ 0.3 mm $\times$ 0.1 mm in 14 days from solutions of 100 mM Tris-HCl (pH 8.5), 200 mM sodium acetate, and 30% PEG 4000 (phosphate-free as shown by the Malachite Green phosphate assay). Crystals for data collection were frozen in 100% Paratone-N (Hampton Research) directly in a stream of nitrogen gas cooled by liquid nitrogen. Diffraction data were collected at $-$180 °C to 1.70 Å resolution using Cu Kα radiation from a Rigaku RU-300 generator equipped with the R-Axis IV^{++} image plate (Boston University School of Medicine). Data were indexed and scaled using DENZO and SCALEPACK (*51*). Data collection statistics are summarized in Table 1. Phases were solved via the molecular replacement program Molrep (*52*) using the model of phospho-β-PGM (PDB entry 1LVH) (*43*). The program yielded an initial solution with a correlation coefficient of 25% and an *R*-factor of 54%. The model was refined using successive rounds of manual rebuilding in the molecular graphic program O (*53*) followed by minimization and simulated annealing in CNS (*54*) using an MLF target function with data from 100 to 1.90 Å. To avoid model bias, metal cofactors and waters were added when R_{free} (*55*) was less than 30%. Refinement and final model statistics are summarized in Table 1. The coordinates are listed in the Protein Data Bank as entry 1ZOL.

β-PGM Site-Directed Mutants

Mutagenesis was carried out using a two-step PCR strategy with the wild-type P71447/pET3a plasmid as the template, primers custom synthesized by Invitrogen, the PCR kit supplied by Stratagene, and the Techgene thermal cycler manufactured by TECHNE (Princeton, NJ). The PCR products were digested with restriction enzymes *Nde*I and *Bam*HI (from New England Biolabs) and ligated to a pET3a vector digested by the same restriction enzymes. The ligation products were used directly to transform *E. coli* BL21(DE3) competent cells (Novagen). The sequence of the mutated gene was confirmed by DNA sequencing at the Center for Genetics in Medicine, University of New Mexico. The D8A, D8E, D170A, and E169A/D170A mutant proteins were purified as described above for the wild-type protein (*15*) and shown to be homogeneous by SDS$-$PAGE gel analysis. The yields of the mutant proteins ranged from 2 to 4 mg/g of wet cells.

Table 1: Crystallographic Data Collection and Model Statistics

data collection statistics	
space group	$P2_12_12_1$
unit cell dimensions	a = 52.760 Å, b = 57.190 Å, c = 75.640 Å
X-ray source	Cu Kα
resolution range (Å)	18.9$-$1.9
highest-resolution shell (Å)	1.97$-$1.90
no. of total/unique reflections	264222/18653
completeness (%)	98.6 (96.7)[a]
$I/\sigma(I)$	15.4 (5.4)[a]
R_{merge} (%)	3.8 (13.7)[a]
volume fraction of protein (%)	54.2
data redundancy	2.4 (2.4)[a]
refinement statistics	
resolution range (Å)	18.9$-$1.9
no. of protein atoms/asymmetric unit	1707
no. of waters/asymmetric unit	288
no. of Mg(II) ions/asymmetric unit	1
no. of total reflections (working set/free set)	18357/1808
R_{work}/R_{free} (%)	20.2/21.1
Ramachandran plot	
residues in most favored regions (%)	94.9
residues in additionally allowed regions (%)	5.1
average *B*-factor (Å^2)	24.1
average of all amino acids	24.5
average of Mg^{2+} atoms	22.3
average of solvent	35.4
average of main chain atoms	21.0
average of side chain atoms	24.9
Luzzati coordinate error (Å)	0.21
rmsd	
bond lengths (Å)	0.011
dihedrals (deg)	23.00
angles (deg)	1.50
impropers (deg)	1.58

[a] Values in parentheses are those for the highest-resolution shell (2.0$-$1.9 Å).

Steady-State Kinetic Experiments

Kinetic Assays. All kinetic assays were carried out at 25 °C in 50 mM K$^+$Hepes (pH 7.0) containing 2 mM $MgCl_2$, unless stated otherwise. The formation of G6P was monitored by measuring the increase in solution absorbance at 340 nm ($\Delta\epsilon$ = 6.2 mM^{-1} cm^{-1}) resulting from the G6P dehydrogenase-catalyzed reduction of NADP.[2] A typical β-G1P to G6P conversion reaction would be carried out by adding a specified volume of a β-PGM stock solution to a 1 mL solution containing known concentrations of α-G16P and β-G1P in 50 mM K$^+$Hepes (pH 7.0), 2 mM $MgCl_2$, 0.2 or 0.4 mM NADP, and 3 units/mL G6P dehydrogenase.

[2] Glucose-6-phosphate dehydrogenase recognizes the β-G6P epimer as the substrate (*1*, *2*). However, the solution epimerization of the C(1)-OH group of G6P is fast because of the intramolecular acid$-$base catalysis of mutarotation in glucose (*3*) offered by the C(6) phosphoryl group (*4*). Fast mutarotation allows the dehydrogenase to be used as a coupling enzyme to detect G6P formed from mutase catalysis of α-G1P and β-G1P (*5*).

The formation of glucose was monitored by measuring the increase in solution absorbance at 340 nm ($\Delta\epsilon = 6.2$ mM^{-1} cm^{-1}) resulting from the glucose dehydrogenase (10 units/mL)-catalyzed reduction of NADP (0.5 mM).

Mg^{2+} Activation. A β-PGM stock solution (20 mg/mL) was dialyzed first against three changes of 50 mM K^+Hepes (pH 7.2) containing 20 mM EDTA and 1 mM DTT and then against 50 mM K^+Hepes (pH 7.2) with 1 mM DTT. The initial velocity of G6P formation in reaction solutions initially containing 3 units/mL G6P dehydrogenase, 200 μM NADP, 50 μM α-G16P, 50 μM β-G1P, 0.02 μM metal-free βPGM, and 0−1.2 mM $MgCl_2$ in 1 mL of 50 mM K^+Hepes (pH 7.0 and 25 °C) was determined by monitoring the absorbance increase at 340 nm ($\Delta\epsilon = 6.2$ mM^{-1} cm^{-1}). The kinetic data were analyzed using eq 1 and the computer program of Cleland (*56*).

$$V_0 = V_m[A]/(K_m + [A]) \quad (1)$$

where [A] is the $MgCl_2$ concentration, V_0 is the initial velocity, V_m is the maximum velocity, and K_m is the Michaelis constant for Mg^{2+} activation. The k_{cat} was calculated from the ratio of V_{max} to the enzyme concentration.

pH−Rate Profiles. The steady-state kinetic constants k_{cat} and K_m for the β-PGM-catalyzed conversion of β-G1P to G6P were measured in the pH range of 4.5−9.0 by measuring the initial reaction velocity as a function of β-G1P concentration in the range of 0.5−10K_m. The following buffers were employed at a concentration of 50 mM for the indicated pH range: sodium acetate for pH 4.50−5.50, K^+Mes for pH 5.50−7.00, K^+Hepes for pH 6.75−8.25, Tris-HCl for pH 8.15−9.00, and K^+Ches for pH 9.00−9.50. All buffers contained 2 mM $MgCl_2$ at a constant ionic strength (adjusted by adding KCl). α-G16P, NADP, and G6P dehydrogenase were maintained at saturating levels to ensure that β-PGM catalysis was rate-limiting. Buffer inhibition was checked at overlapping pH values. The k_{cat} and K_m values were determined from the initial velocity data using eq 1 where [A] is the β-G1P concentration. The k_{cat} was calculated from the ratio of V_{max} to the enzyme concentration. The pH−rate profiles were fitted using eqs 2−4 and the computer programs of Cleland (*56*).

$$\log Y = \log\{C/[1 + H/K_{a1} + H \times H/(K_{a1}K_{a2})]\} \quad (2)$$

$$\log Y = \log[C/(1 + K_b/H)] \quad (3)$$

$$\log Y = \log[C/(1 + K_{b1} \times K_{b2}/H \times H)] \quad (4)$$

where Y is k_{cat} or k_{cat}/K_m, C is a pH-independent value of k_{cat} or k_{cat}/K_m, H is the proton concentration, and K_a and K_b are ionization constants.

Activation by Phosphorylation. The steady-state kinetic constants for β-PGM activation by phosphorylation were measured by varying the concentration of the activator between 0.5 and 5 times K_m at a fixed (50 μM) β-G1P concentration in 50 mM K^+Hepes (pH 7.0) containing 0.004 μM β-PGM, 2 mM $MgCl_2$, 0.2 mM NADP, and 3 units/mL G6P dehydrogenase. Data were fitted to eq 1 (where [A] is the activator concentration) to obtain k_{cat} and K_m. Alternatively, the kinetic determinations were carried out at varying β-G1P concentrations (0.5−5K_m), and data were computer fitted (*56*) to eq 5.

$$V_0 = V_m[A][B]/(K_B[A] + K_A[B] + [A][B]) \quad (5)$$

where [A] is the activator concentration, [B] is the β-G1P concentration, V_0 is the initial velocity, V_m is the maximum velocity, K_A is the Michaelis constant for the activator, and K_B is the Michaelis constant for the β-G1P. The k_{cat} was calculated from the ratio of V_{max} to the enzyme concentration.

β-PGM-Catalyzed Acetyl Phosphate Hydrolysis. β-PGM (20 μM) was preincubated with acetyl phosphate (0.5, 1, or 5 mM) in 50 mM K^+Hepes (pH 7.0 and 25 °C) containing 2 mM $MgCl_2$. At varying incubation periods, a 5 μL aliquot of the solution was removed and added to a 1 mL assay solution which contained 100 μM β-G1P, 2 mM $MgCl_2$, 3 units/mL G6P dehydrogenase, and 400 μM NADP in 50 mM K^+Hepes (pH 7.0 and 25 °C). The initial velocity of G6P formation was determined from the rate of the increase in solution absorbance at 340 nm ($\Delta\epsilon = 6.2$ mM^{-1} cm^{-1}) and plotted as a function of the time period of incubation of β-PGM with acetyl phosphate.

Inhibition Experiments. The 1 mL assay solutions used in the inhibition experiments initially contained 0.004 μM β-PGM, 50 μM α-G16P, 5−200 μM β-G1P, 2 mM $MgCl_2$, 200 μM β-NADP, 2.5 units of G6P dehydrogenase, and varying concentrations of sodium tungstate (0, 125, 250, and 500 μM) or molybdate (0, 160, and 320 μM) in 50 mM K^+-Hepes (pH 7.0). The inverse of the initial velocity was plotted as a function of the inverse of the β-G1P concentration for each inhibitor concentration to form a set of parallel lines. The intercepts ($1/V_{max}$) of these plots were then plotted as a function of inhibitor concentration to form a parabola.

p-Nitrophenyl Phosphate Assay. Reaction solutions (1 mL) initially containing 2 μM β-PGM, varying concentrations of *p*-nitrophenyl phosphate (5−100 mM), 2 mM $MgCl_2$, and 50 mM K^+Hepes (pH 7.0 and 25 °C) were monitored at 410 nm ($\Delta\epsilon = 18.4$ mM^{-1} cm^{-1}). The initial velocity data were analyzed using eq 1.

Single-Turnover Kinetic Experiments

Reaction solutions (28 μL) initially containing 40 μM β-PGM or the sugar-phosphate phosphatase BT4131 (from the bacterium *B. thetaiotaomicron* VPI-5482), 5 μM [^{14}C]-D-glucose 6-phosphate (SA = 49.3 mCi/mmol), 2 mM $MgCl_2$, and 50 mM K^+Hepes (pH 7.0 and 25 °C) were incubated for a specified period and then the reactions quenched with 160 μL of 0.6 M NaOH. The resulting mixture was passed through a 5 kDa filter to remove the enzyme, and then chromatographed with a Rainin Dynamax HPLC system equipped with a CarboPac PA1 Dionex (4 mm × 250 mm) column. The column was eluted at flow rate of 1 mL/min, first with 2 mL of solvent A (54 mM NaOH and 100 mM sodium acetate), then with a linear gradient (15 mL) of solvent A to 53.7% solvent B (75 mM NaOH and 500 mM sodium acetate), and finally with solvent B. Fractions (1 mL) were collected and their radioactivities determined by liquid scintillation counting. The radioactivity was used to calculate the concentration of [^{14}C]glucose (retention time of 3 min) and [^{14}C]G6P (retention time of 15 min) present in the reaction mixture at the time of quenching, by multiplying the initial G6P concentration by the fraction of the total radioactivity. No [^{14}C]G1,6bisP

(retention time of 21 min) was detected in the quenched reaction mixture.

RESULTS AND DISCUSSION

Crystal Structure of the β-PGM−Mg^{2+} Complex. The crystal structure of the Mg^{2+} complex of *L. lactis* β-PGM was determined to 1.9 Å resolution. The structure reveals the relative orientation of the cap domain with respect to the core domain to be in the "open conformation" previously observed for the Mg^{2+} complex of phosphorylated β-PGM (phospho-β-PGM) (C_α rmsd of 1.22 Å) (*43*). In this conformation, the core domain active site is exposed to solvent. In contrast, the X-ray structures reported for the β-PGM−β-glucose-6-phosphate-1-phosphorane−Mg^{2+} complex (*44*) and the β-PGM−α-galactose 1-phosphate−Mg^{2+} complex (*58*) display the cap domain relative to the core domain to be in the "closed conformation". In this "catalytically active" conformation, the core domain active site is solvent inaccessible. The superposition of the structure of the β-PGM−Mg^{2+} complex on the structure of the β-PGM−β-glucose-6-phosphate-1-phosphorane−Mg^{2+} complex (*44*) illustrates the change in conformation which takes place following binding of the β-G16P ligand to the free enzyme (see Figure 2A). Whereas the intradomain conformational changes are small [the two domains that comprise the enzyme can be superimposed with a low rmsd of 0.88 $Å^2$ (cap) and 0.77 $Å^2$ (core) for C_α atoms], the interdomain conformational changes are large. Domain−domain closure is accomplished by the rigid motion of the "cap" domain (residues 16−78) relative to the "core" domain along an effective hinge axis by 26° as calculated by DynDom (*57*). The movement of the cap domain brings the cap residue, Arg49, within hydrogen-bond forming distance of the C(6) phosphoryl group of G16P (see Figure 2B), while sealing the active site to solvent (*44*).

The structure of the phospho-β-PGM−Mg^{2+} complex (C_α trace not shown, but essentially the same as that of the β-PGM−Mg^{2+} complex shown in Figure 2A) provides a snapshot of the enzyme following phosphoryl transfer from the G16P ligand to the Asp8 and subsequent release of the G6P product. The cap and core domains have dissociated, thereby opening the active site to solvent. One would anticipate that β-G1P binds to this form of the enzyme, and that the cap and core domains once again associate to close the active site for catalysis. Indeed, the crystal structure of the α-D-galactose 1-phosphate-bound β-PGM−Mg^{2+} complex, in which the C(1) phosphate is bound in the "non-transferring" phosphate binding site distal to Asp8, shows the enzyme to be in the closed conformation (*58*) with the cap domain Arg49 positioned to form a hydrogen bond with the ligand C(1) phosphate (see Figure 2B for the position of Arg49).

On the basis of these crystallographic snapshots, we surmise that during its catalytic cycle, β-PGM exchanges ligands by opening the core domain active site to solvent via cap domain dissociation. Thus, in the cartoon shown in Figure 2C, we depict β-PGM as a "feeding clam" (Figure 2C), opening its active site to bind the β-G16P phosphoryl donor, closing to allow autophosphorylation, opening to release the G6P product and absorb the β-G1P substrate, and then closing once again for phosphoryl transfer to take place before opening to release β-G16P.

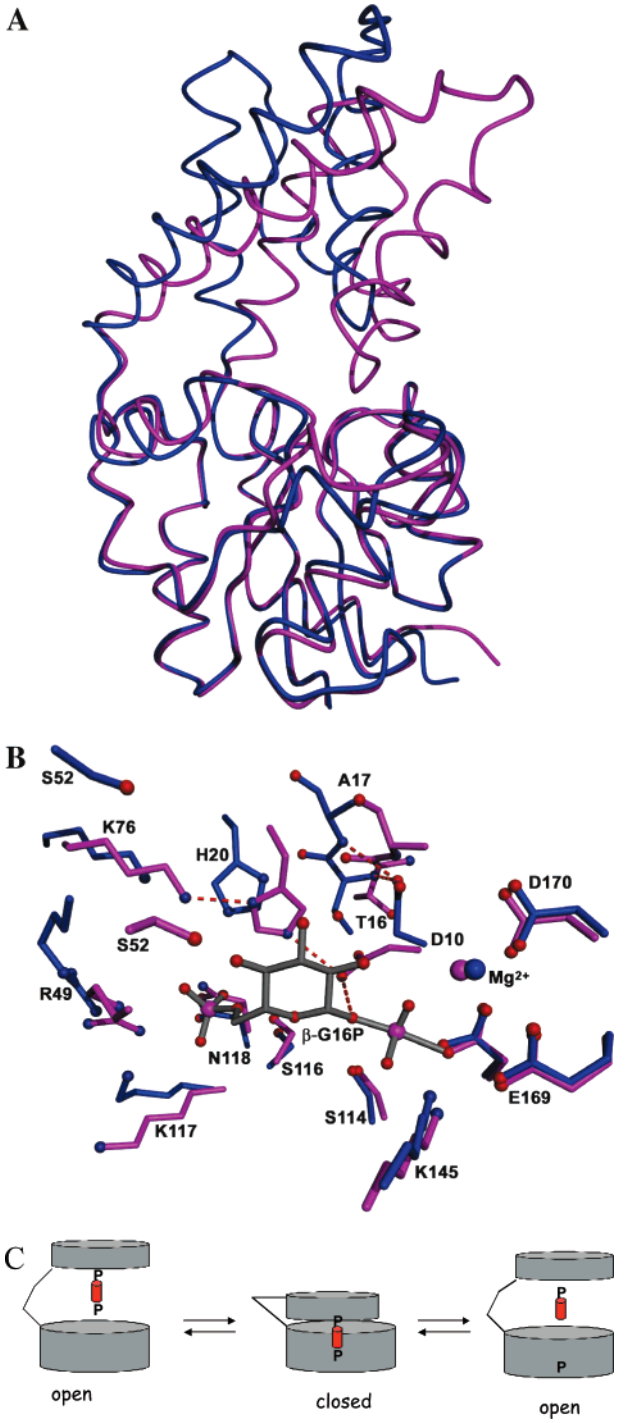

FIGURE 2: (A) Overlay of the backbone (blue) of the β-PGM−Mg^{2+} complex with the backbone (pink) of the β-PGM−Mg^{2+}−6-phosphoglucose-1-phosphorane complex. (B) Overlay of the active sites of the β-PGM−Mg^{2+} complex (blue) and the β-PGM−Mg^{2+}−6-phosphoglucose-1-phosphorane complex (protein in pink and phosphoglucose in gray). S52, K79, H20, and R49 belong to the cap domain. T16 and A17 are the hinge residues. D10 is the acid−base catalyst, which along with S116, S114, K117, N118, K145, E169, and D170 is derived from the core domain. The Mg^{2+} is represented as a sphere colored the same as the backbone of the corresponding structure. Water ligands have been omitted for clarity. Unique hydrogen bonds to each structure are depicted as dashed lines colored the same as the backbone of the corresponding structure. (C) Cartoon depicting the enzyme conformational changes expected to occur along the reaction pathway.

In contrast to the domain movements suggested by these crystal structures, the core domain active site residues stay

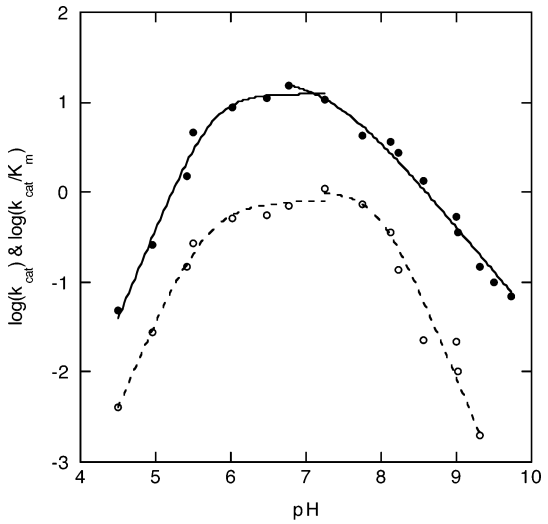

FIGURE 3: Plots of log k_{cat} (●) and log k_{cat}/K_m (○) vs pH measured for the β-PGM-catalyzed conversion of βG1P to G6P. Ascending and descending regions of the plots were separately fitted with equations describing one or two ionizations. See Materials and Methods for details.

fixed. The single exception to this rigid catalytic template is Asp10. As shown in Figure 2B, in the cap open conformation, the side chain of Asp10 is engaged in hydrogen-bond formation with the backbone amide NH groups of Thr16 and Ala17 and is, thus, directed away from the reaction center. These two residues form the hinge region of interdomain peptide linker 1. In the β-PGM−β-glucose-6-phosphate-1-phosphorane−Mg^{2+} complex, the backbone conformation at the hinge has changed, and the Asp10 side has rotated into the active site where it forms a hydrogen bond with the ligand C(1)O and with the cap domain His20, which has also entered the active site. By coupling cap closure to ligand binding [a common feature among the two-domain HAD phosphotransferases (*59*)], and acid−base catalysis via Asp10 to cap closure, phospho-β-PGM can discriminate between β-G1P and water as the phosphoryl group acceptor. In this study, the level of discrimination between phosphoryl group acceptors was measured as described below.

pH Dependence of β-PGM Catalysis. L. lactis β-PGM was reported to be relatively stable in solution within the pH range of 5−9.5, but to have a comparatively narrow pH range for catalysis based on velocity measurements taken at several pH values (*6*). Here we examine the pH dependency of *L. lactis* β-PGM catalysis using the log k_{cat} and log k_{cat}/K_m versus pH profiles of β-PGM-catalyzed conversion of βG1P to G6P to define apparent pK_a values of essential residues. The profiles obtained were bell-shaped and defined optimal catalytic functioning at or near neutral pH. As shown in Figure 3, the data defining the acid and base regions of the pH−rate profiles were fitted to equations defining one or two ionizations (see Materials and Methods) to obtain apparent pK_a values for the ionizing groups. The acid range of the log k_{cat} profile defines two essential base residues, the conjugate acids of which ionize with apparent pK_a values of 4.7 and 6.7. The alkaline range of the log k_{cat} profile defines one essential acid residue that ionizes with an apparent pK_a value of 7.3. The acid region of the log k_{cat}/K_m profile defines two essential base residues that, as conjugate acids, ionize with apparent pK_a values of 5.5 and 5.8. The base pH range of the log k_{cat}/K_m profile defines two essential acid residues that ionize with an average apparent pK_a value of 7.9. No attempt has yet been made to assign these ionizations to active site residues, but this goal will be undertaken in the future. At this juncture, the pH−rate profile analysis identified pH 7.0 as the optimal pH at which to carry out the β-PGM kinetic experiments described below.

Mg^{2+} Site of β-PGM. Comparison of the Mg^{2+} sites (Figure 4) observed in the structures of the free β-PGM ("E"), phospho-β-PGM ("E−P"), and the β-PGM−β-glucose-6-phosphate-1-phosphorane complex ("E−P−GP") reveals that the Mg^{2+} ligands derived from the enzyme core domain are retained throughout the catalytic cycle. In each enzyme complex, the Mg^{2+} is coordinated by the Asp8 and Asp170 side chains and the Asp10 backbone carbonyl oxygen. In the active site of E, there are three ordered water molecules, labeled Wat1−Wat3 (Figure 4A), that occupy the remaining coordination positions of the Mg^{2+}. Each of the three water ligands engages in hydrogen bond interactions with surrounding residue side chains: Wat1 with Glu169 (2.5 Å), Asp170 (3.1 Å), and Ser171 (2.7 Å); Wat2 with Asp8 (3.1 and 2.9 Å); and Wat3 with Asp10 (2.7 Å) and Asp170 (2.7 and 3.2 Å). In the E−P and E−P−GP complexes, Wat1 and Wat3 are retained but Wat2 is replaced with the Asp8 phosphoryl group, which in the E−P complex is tetrahedral at the phosphate phosphorus and in the E−P−GP complex trigonal bipyramidal at phosphorus (Figure 4B). The Mg^{2+} of the free enzyme is only slightly distorted from a perfect octahedral geometry with the nucleophilic Asp8 ligand, 81° from the plane of the bipyramid (the ideal is 90°). There is a small but significant 0.6 Å shift (compared to the 0.21 Å coordinate error of the structure) in the position of the Mg^{2+} observed in the free enzyme versus the E−P and E−P−GP complexes.

The Mg^{2+} activation constant was determined by measuring the dependence of the initial velocity of the β-PGM-catalyzed conversion of β-G1P to G6P on the concentration of added Mg^{2+}. The plot shown in Figure 5 defines an apparent K_m for Mg^{2+} of 270 ± 20 μM.[3] The low Mg^{2+} binding affinity of β-PGM contrasts the high Mg^{2+} binding affinity observed with a close structural homologue, phosphonatase (*61*). In phosphonatase, the Mg^{2+} cofactor is bound so tightly (K_d < 1 μM) that it cannot be removed by dialysis without denaturing the enzyme (*60*). The constellation of Mg^{2+} ligands in these two HAD family enzymes is conserved, while the Mg^{2+} binding affinity has diverged.

Here we examine the contribution made by the metal binding loop in β-PGM, and compare it with that of phosphonatase. The seven-stationed HAD family metal binding loop positions two carboxylate residues for Mg^{2+} binding (*60*). Both β-PGM and phosphonatase position the inner-sphere Mg^{2+} ligand (Asp170 in β-PGM and Asp186 in phosphonatase) at station 3. Whereas Ala substitution for Asp186 in phosphonatase precludes catalytic turnover (*60*), Ala substitution for Asp170 in β-PGM does not. The β-PGM D170A mutant is impaired but active, with a k_{cat} of (3.84 ± 0.03) × 10^{-3} s^{-1} and a K_m of 7.8 ± 0.2 μM (Table 2). In

[3] Previous studies of *L. lactis* β-PGM metal ion activation indicated a Mg^{2+} K_m of ~1 mM, but this measurement was taken in the presence of Triton X-100 (*6*). Also, it is noted here that because metal binding is at thermodynamic equilibrium, the K_m of activation is a measure of the binding affinity between the enzyme and the Mg^{2+}.

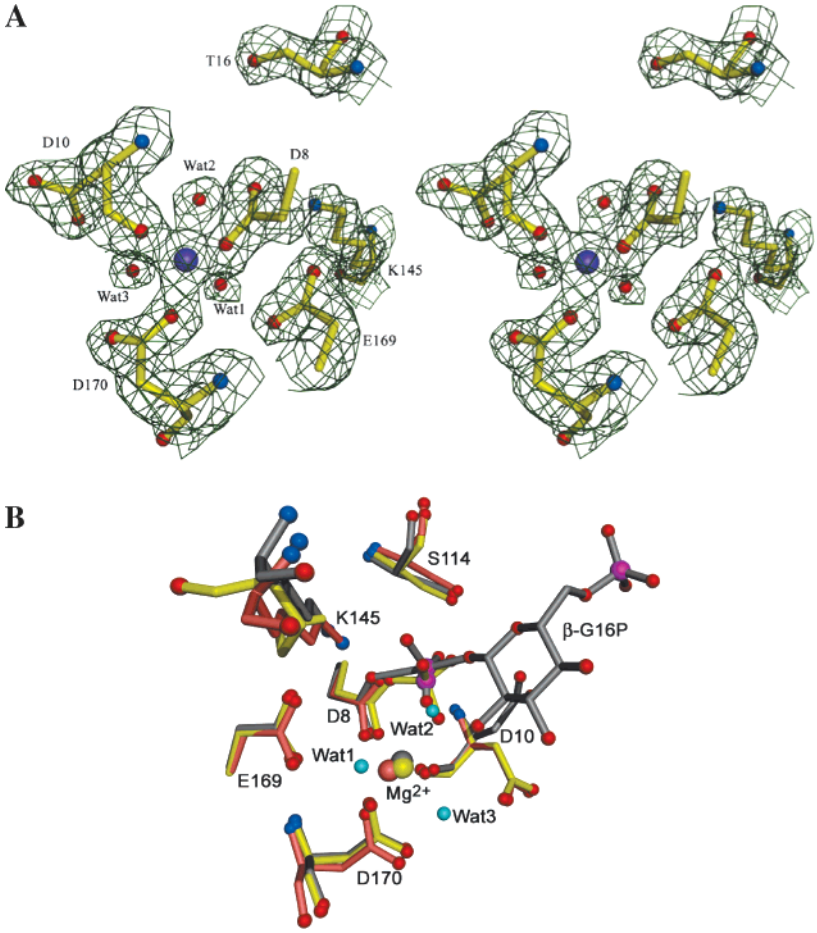

FIGURE 4: (A) Electron density map ($2F_o - F_c$) contoured at 1.5σ of the Mg^{2+} binding site of the β-PGM−Mg^{2+} complex. (B) Overlay of the Mg^{2+} binding sites observed in the structures of the β-PGM−Mg^{2+} (pink), phospho-β-PGM−Mg^{2+} (yellow), and β-PGM−Mg^{2+}−6-phosphoglucose-1-phosphorane (gray) complexes. Waters are depicted as cyan spheres, and Mg^{2+} is depicted as a sphere colored the same as the backbone of the corresponding structure.

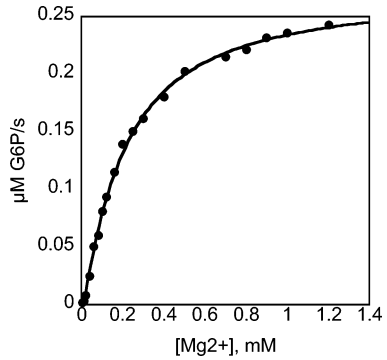

FIGURE 5: Plot of initial velocity of the βPGM-catalyzed conversion of βG1P to G6P vs Mg^{2+} concentration. Reaction mixtures contained 3 units/mL G6P dehydrogenase, 200 μM NADP, 50 μM α-G16P, 50 μM β-G1P, 0.02 μM metal-free β-PGM, and 0−1.2 mM $MgCl_2$ in 50 mM K^+Hepes (pH 7.0 and 25 °C).

Table 2: Kinetic Constants for Wild-Type and Mutant β-PGMs (in the presence of 50 μM α-G16P as the activator)

enzyme	$K_{m-Mg^{2+}}$ (μM)	K_{m-G1P} (μM)	k_{cat} (s^{-1})
wild type	270 ± 20	14.6 ± 0.5	17.1 ± 0.6
D8A	inactive		
D8E	inactive		
D170A	not determined	7.8 ± 0.2	(3.84 ± 0.03) × 10^{-3}
E169A/D170A	not determined	390 ± 20	(1.20 ± 0.02) × 10^{-3}

HAD phosphotransferases, the "other" carboxylate residue stationed on the metal binding loop binds the Mg^{2+} through hydrogen-bond formation with its water ligand. Glu169 of β-PGM is located on station 2, while Asp190 of phosphonatase is located at station 7. Replacement of Asp190 with Ala reduces the k_{cat} of phosphonatase 700-fold (*60*) and increases the substrate K_m ~200-fold, and the Mg^{2+} K_m ~1000-fold (K_m = 3.5 mM). On the other hand, retention of catalytic activity in the β-PGM E169A/D170A double mutant [k_{cat} = (1.20 ± 0.02) × 10^{-3} s^{-1} and K_m = 390 ± 20 μM] suggests that the Asp8 carboxylate group, together with the backbone carbonyl of Asp10 (ligands seen in the X-ray structure), can secure the cofactor. Compared to the metal binding loop of phosphonatase, the metal binding loop of β-PGM makes a smaller contribution to the binding of Mg^{2+}. As can be seen in the overlay in Figure 4B, water, phosphate, and phosphorane oxygen ligands exchange for a single Mg^{2+} coordinate site. It is tempting to speculate that the loose grip imposed by the β-PGM metal binding loop might allow the Mg^{2+} to shift as needed to accommodate the different phosphate ligands encountered during a catalytic cycle.

The Nucleophile Asp8 Is Essential for Catalysis. The X-ray crystal structure of phospho-β-PGM shows that the site of phosphorylation is Asp8 (*43*). This active site residue is invariant in the HAD superfamily, where, within the haloalkonate dehalogenase branch, it is known to function in nucleophilic catalysis by displacing the halide from the

2-haloalkonoate substrate to form an alkylated enzyme intermediate (*62*). The participation of the invariant Asp in mediation of phosphoryl transfer has been implicated by retention of phosphorus stereochemistry (*63*, *64*) and by Asp−BeF_3 adduct formation in the protein crystal (*65*, *66*). In addition, several papers have reported ^{32}P labeling of a HAD family phosphotransferase using ^{32}P-labeled substrate and/or chemical trapping of the aspartyl phosphate residue (*67*−*73*).

Despite all this evidence, we sought further proof that Asp8 functions in nucleophilic catalysis. From recently reported studies of *P. aeruginosa* α-PGM/α-PMM (*32*, *33*), we learned that the S108A mutant retains 12% activity, despite the fact that Ser108 has been shown to be the site of phosphorylation (*13*). Furthermore, the S108A mutant is phosphorylated by the G16P activator (*33*). These observations warn that suspected nucleophilic catalysis should be verified by site-directed mutagenesis experiments. Accordingly, Asp8 of β-PGM was mutated and the activity of the mutants measured. Here, we report that the D8A and D8E β-PGM mutants are inactive as determined by an assay that measures residual activity to a minimal turnover rate of 1×10^{-5} s^{-1}. Both mutants were judged to possess native structure on the basis of the criteria of yield, solubility, stability, and chromatographic behavior. Therefore, we conclude that Asp8 plays an essential role in β-PGM catalysis.

It is curious that the β-PGM Asp8 nucleophile is essential to catalysis but the α-PGM/α-PMM Ser108 nucleophile is not. For β-PGM, the structure of the β-glucose-6-phosphate-1-phosphorane−Asp8 complex is strong evidence for an associative mechanism in which Asp8 attacks the phosphorus prior to leaving group departure (*44*). An intriguing possibility for the PGM/α-PMM is that the highly electrostatic environment of the desolvated active site (*13*, *14*) might support a metaphosphate intermediate (*74*), which preferentially docks at Ser108 or the C(6)OH group of αG1P.

β-PGM Activation by Phosphorylation. Having established that β-PGM is phosphorylated at Asp8, we next sought to identify the physiological β-PGM phosphorylating agent. For *L. lactis* β-PGM to efficiently catalyze the conversion of β-G1P to G6P, it requires an activator, a requirement conveniently met in the laboratory by commercial α-G16P (*39*).[4] Here, we examine the specificity of β-PGM autophosphorylation by comparing activation by α-G16P to activation by known phosphorylated metabolites by using steady-state kinetic methods. The phosphoryl donor and the β-G1P bind to separate enzyme forms (E and E−P, respectively), giving rise to parallel-patterned double-reciprocal plots (i.e., inverse velocity vs inverse β-G1P concentration measured at a changing, fixed activator concentration). In short, β-PGM activation conforms to a bi-bi ping-pong mechanism as illustrated by the kinetic plot measured with α-G16P (Figure 6A). Data fitting defined a k_{cat} of 17 s^{-1} and a K_m of 20 μM for the activator α-G16P. When this kinetic experiment was repeated with α-D-fructose 1,6-(bis)phosphate (α-F16P), a K_m of 100 μM and a k_{cat} of 17 s^{-1} were obtained (Figure 6B). Finally, the kinetic experiment was carried out with acetyl phosphate serving as the activator, to obtain the plot shown in Figure 6C. Because of the high saturation threshold, the steady-state kinetic constants ($k_{cat} = 16.6 \pm 0.3$ s^{-1} and $K_m = 800 \pm 30$ μM) for acetyl phosphate were derived from a separate set of initial velocity data measured over a range of 0.30−3.2 mM acetyl phosphate concentrations at a fixed β-G1P concentration (50 μM). ATP (10 mM), which has been implicated in the autophosphorylation of α-PGM (*22*), had no effect on β-PGM catalysis, either as an activator or as an inhibitor. Likewise, orthophosphate (10 mM) did not activate or inhibit the enzyme in solution (but see Observation of Phospho-β-PGM in the Crystal).

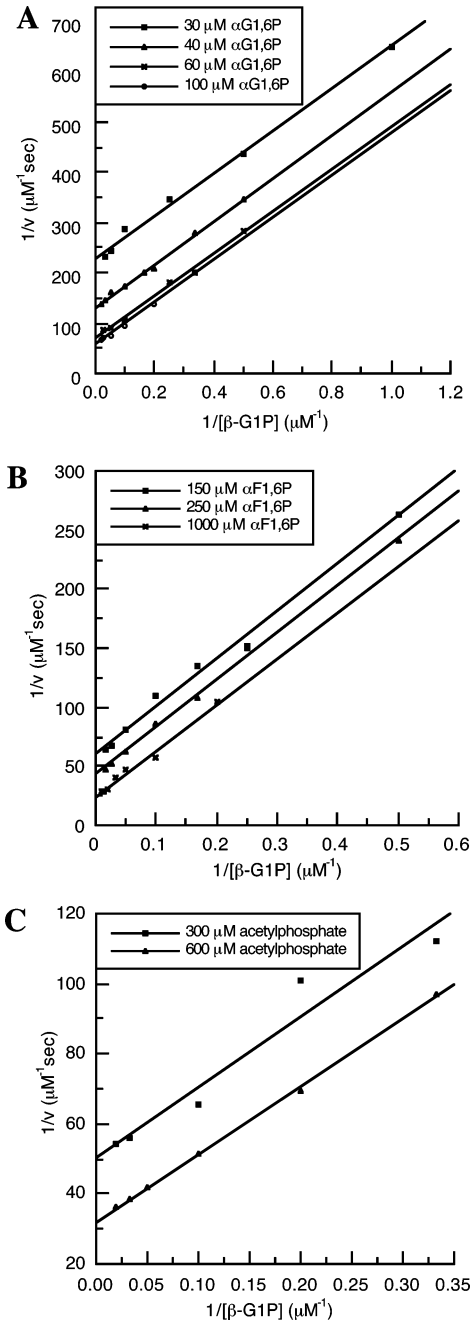

FIGURE 6: Plots of inverse velocity vs inverse β-G1P concentration measured at various, fixed phosphoryl donor concentrations (as shown in the boxed insets) using (A) α-G16P, (B) α-F16P, and (C) acetyl phosphate as activators.

[4] β-G16P is not commercially available. However, by isolating it as a minor contaminant in their synthetic β-G1P preparation, Belocopitow and Marechal measured the K_m (0.5 μM) for β-G16P activation of *E. gracilis* β-PGM (*42*).

These results show that once secured in the β-PGM active site, the various phosphoryl donors are equally reactive (i.e., k_{cat} values are equivalent). Activator specificity is based on "apparent" binding affinity, which is 5-fold higher for α-G16P compared to α-F16P and 40-fold higher for α-G16P compared to acetyl phosphate. The apparent binding affinity is determined by favorable interaction with residues contributed by the core and cap domains.

We have concluded that phosphoryl transfer from the α-G16P (and similarly from the α-F16P) occurs from the C(6) position.[5] This conclusion is based on two observations. First, β-PGM, activated with 50 μM α-G16P, catalyzes the conversion of β-G1P to G6P ($k_{cat} = 17.1 \pm 0.6$ s^{-1}; β-G1P $K_m = 14.6 \pm 0.5$ μM) but not the conversion of α-G1P to G6P. Specifically, no product was detected in the mixture of 10 μM β-PGM, 100 μM α-G16P, and 300 μM α-G1P in 2 mM $MgCl_2$ and 50 mM K^+Hepes (pH 7.0) following incubation for 1 h at 25 °C. Thus, phosphoryl transfer cannot occur from C(1) in the α-isomer of G1P, and by analogy from C(1) of α-G16P. Transfer must instead occur from C(6) of α-G16P. Second, on the basis of the X-ray crystal structure of the *L. lactis* β-PGM complexed with the inhibitor α-D-galactose 1-phosphate (*58*), we can assume that the C(1) phosphate of α-G16P will bind to the distal nontransferring phosphate binding site where it serves to stabilize the closed conformation of the active site (*44*). Thus, whereas the epimer specificity at the transferring phosphate site is high, at the distal phosphate site it is lax.

Unlike α-G16P and α-F16P, acetyl phosphate does not possess a phosphoryl group to bind to the distal phosphate-binding site. As a consequence, it is unable to stabilize the closed conformation by interaction with the cap domain Arg49. Thus, acetyl phosphate binding cannot trigger the release of the Asp10 carboxylate from hinge residues Thr16 and Ala17, to participate in acid catalysis (see Figure 2B). However, because of the low energy of the acetate-leaving group, phosphorylation of the Asp8 is not impeded. As will be shown below, this is not the case for β-G1P, which is the most logical choice for the native β-PGM activator.

In *L. lactis*, β-G1P is formed when maltose is degraded by the action of maltose phosphorylase (*76*). Both maltose phosphorylase and β-PGM synthesis are induced by maltose (*75*). Thus, the appearance of β-PGM coincides with that of β-G1P. Mesak and Dahl (*40*) have suggested that because β-PGM from *B. subtilis* displays high β-G1P dismutase activity, it might synthesize its activator by autophosphorylation. Accordingly, we tested *L. lactis* for β-G1P dismutase activity. The β-PGM turnover rate for glucose formation in a reaction mixture initially containing 10 μM β-PGM, 0.5 mM β-G1P, 0.5 mM NADP, 10 units/mL glucose dehydrogenase, 2 mM $MgCl_2$, in 50 mM K^+Hepes (pH 7.0 and 25 °C) was measured at 3×10^{-4} s^{-1}. In contrast, for G6P formation, $k_{cat} = 0.83 \pm 0.01$ s^{-1}, and for β-G1P, $K_m = 400 \pm 40$ μM. In the presence of 50 μM α-G16P, G6P is formed with a k_{cat} of 17.1 ± 0.6 s^{-1} and a β-G1P K_m of 14.6 ± 0.5 μM. These results show that β-G1P is a more efficient phosphoryl acceptor (from phospho-β-PGM) than a phosphoryl donor (to β-PGM); i.e., the ratio of k_{cat}/K_m for these two reactions equals 557. Unlike α-G16P or α-F16P, β-G1P does not possess the additional phosphate group which we have hypothesized induces cap closure and, hence, Asp10 acid−base catalysis (vide infra). Consequently, both k_{cat} and K_m for β-G1P activation are less favorable. While the K_m value for β-G1P roughly compares with that of acetyl phosphate (400 vs 800 μM), its k_{cat} value is much smaller (0.8 vs 17 s^{-1}). Unlike acetyl phosphate, β-G1P requires an acid catalyst for protonation at the C(1)O group, and without a phosphoryl group to bind at the distal phosphate binding site, we presume that cap closure, and hence interaction with Asp10, becomes less frequent. Nonetheless, β-PGM autophosphorylation by β-G1P can, in principle, account for the origin of the phospho-β-PGM in the cell.

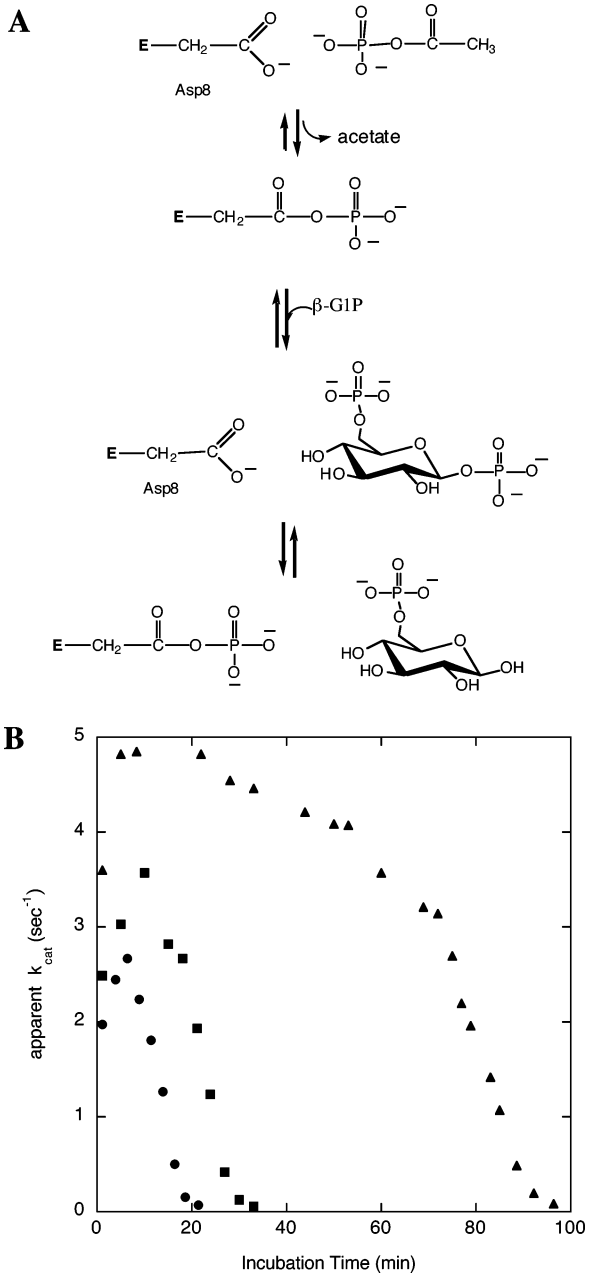

FIGURE 7: (A) Reaction sequence for the phosphorylation of the β-PGM−Mg^{2+} complex with acetyl phosphate followed by reaction of the phospho-β-PGM−Mg^{2+} complex with β-G1P. (B) Plots of β-PGM activity as a function of time of incubation with 0.5 (●), 1 (■), and 5 mM acetyl phosphate (▲) as activators.

[5] In earlier studies, the activation of β-PGM by α-G16P was attributed to the possible contamination of the α-G16P sample by the β-isomer (*39*, *42*, *77*).

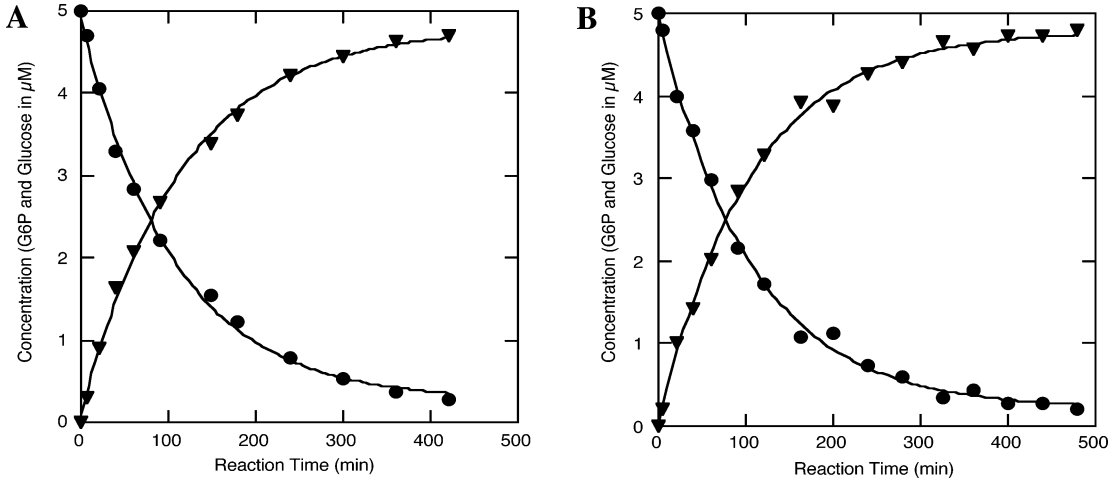

FIGURE 8: Time courses for the consumption of G6P (●) and the formation of glucose (▲) measured in single-turnover reactions of 5 μM [^{14}C]glucose 6-phosphate with 40 μM β-PGM (A) or BT4131 (B) in 50 mM K^+Hepes (pH 7.0 and 25 °C) containing 2 mM $MgCl_2$.

Specificity of Phospho-β-PGM for the Phosphoryl Group Acceptor. β-PGM functions as a mutase rather than as a phosphatase because of its ability to discriminate between water and β-G1P as a phosphoryl group acceptor. Here we report the rate at which phospho-β-PGM transfers its phosphoryl group to water. β-PGM (20 μM) was preincubated with acetyl phosphate (0.5, 1, and 5 mM) in 50 mM K^+Hepes (pH 7.0 and 25 °C) containing 2 mM $MgCl_2$. At varying incubation periods, the reaction mixture was assayed for phospho-β-PGM as detailed in Materials and Methods. The chemical steps anticipated for the preincubation reaction, and the assay reaction, are diagrammed in Figure 7A. The experimental results are plotted in Figure 7B. The time courses for phospho-β-PGM formation and hydrolysis demonstrate that the phospho-β-PGM is not long-lived. The 5 mM acetyl phosphate is consumed in ~80 min, defining a minimum rate for phospho-β-PGM hydrolysis of 3 min^{-1}. This is much faster than the hydrolysis rate k of 2×10^{-6} min^{-1} observed for the phosphoserine group of phospho-α-PGM (*78*). In future studies, the microscopic rate constants for phospho-β-PGM formation and reaction with solvent versus substrate will be determined. However, at this juncture, we can conclude that the phospho-β-PGM phosphoryl transfer to β-G1P ($k_{cat} \sim 20$ s^{-1}) is ~400-fold faster than it is to water. In contrast, in phospho-α-PGM, the α-G1P/water discrimination factor is 3×10^{10} (*78*).

Adaptation of the Core Domain Catalytic Scaffold from Phosphatase to Mutase. The HAD family largely consists of phosphatases whose ability to distinguish between small cellular metabolites is delegated to a cap domain and not to the active site of the core domain (*45*). β-PGM catalysis of acetyl phosphate hydrolysis reflects its ancestry, which is tied to a core domain catalytic scaffold specialized for phosphate ester hydrolysis. Indeed, the core domain of β-PGM is not unlike that of HAD member BT4131 from the bacterium *B. thetaiotaomicron* VPI-5482, which catalyzes the release of phosphate from hexose 6-phosphates and pentose 5-phosphates (*46*). The cap domains of these two enzymes are, however, different in size and topology. Here we compare the abilities of β-PGM and BT4131 to catalyze the hydrolysis of *p*-nitrophenyl phosphate (pNPP), a phosphate ester that does not require acid catalysis. The steady-state kinetic constants measured using 2 μM β-PGM in 2 mM $MgCl_2$ and 50 mM K^+Hepes (pH 7.0 and 25 °C) are as follows: $k_{cat} = (1.78 \pm 0.01) \times 10^{-2}$ s^{-1} and pNPP $K_m = 14.3 \pm 0.3$ mM. For BT4131 in 5 mM $MgCl_2$ and 50 mM K^+Hepes (pH 7.0 and 37 °C), $k_{cat} = (8.3 \pm 0.2) \times 10^{-2}$ s^{-1} and pNPP $K_m = 0.77 \pm 0.05$ mM (*46*). When the temperature difference is included, the k_{cat} values are essentially the same, while the difference in K_m values is consistent with cap-assisted substrate binding in BT4131 but not in β-PGM.

Next, we compared the G6P hydrolase activities of β-PGM and BT4131. The reported steady-state kinetic constants for BT4131-catalyzed hydrolysis of G6P are as follows: $k_{cat} = 3.6 \pm 0.2$ s^{-1} and $K_m = 11 \pm 2$ mM (*46*). To assess the β-PGM-catalyzed hydrolysis of G6P, a single-turnover experiment was carried out to avoid the capture of the phospho-β-PGM by G6P. The time courses measured for the reaction of 40 μM β-PGM or BT4131 with 5 μM [^{14}C]-G6P at 25 °C are shown in Figure 8. Data fitting to a single exponential defines identical pseudo-first-order rate constants[6] for the two reactions: $k_{obs} = 0.0094 \pm 0.0005$ min^{-1}. Thus, the phosphatase activity of the core domain of β-PGM is no different from the phosphatase activity of the core domain of BT4131.

The success of *L. lactis* β-PGM regulation can be attributed to the combination of two factors. First, phospho-β-PGM transfers its phosphoryl group to β-G1P much faster than it does to solvent, and second, the synthesis of β-PGM is induced by maltose (*75*), from which β-G1P is derived (*76*). Thus, unwanted hydrolysis of phosphorylated metabolites by β-PGM is avoided by coordinating the presence of β-PGM with the presence of β-G1P.

By recruiting the cap domain to incorporate a second phosphate-binding site (i.e., the distal phosphate site), β-PGM has evolved from phosphatase to mutase. Indeed, the clear distinction between the phosphohydrolase branch and the mutase branch of the HAD superfamily is that the substrate of the phosphohydrolases is a cognate for the free enzyme while the mutase substrate is a cognate for the phosphoenzyme. This can be demonstrated by the contrasting inhibition

[6] Because of the weak binding of G6P to either enzyme, the concentration of the enzyme−substrate complex present in the reaction mixture is minimal. The prevailing conditions thus approximate a pseudo-first-order reaction.

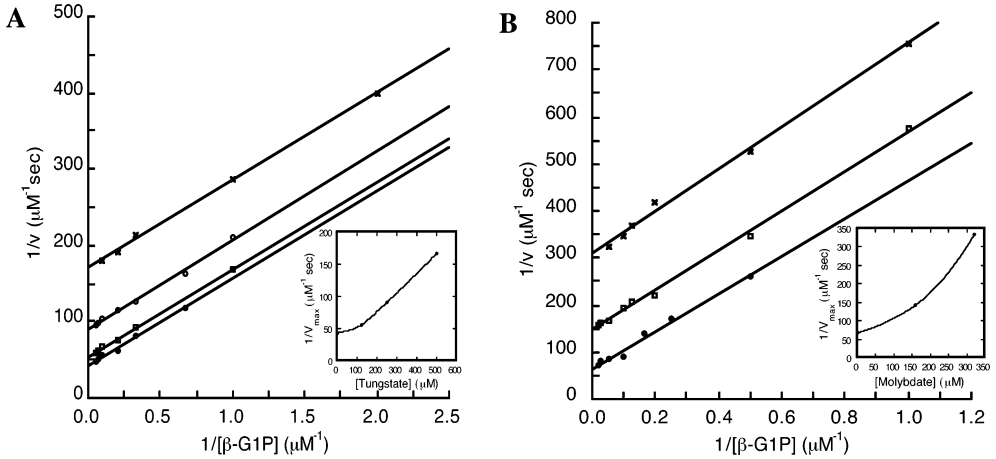

FIGURE 9: Reaction of α-G16P-activated β-PGM with the substrate β-G1P in the presence of 0, 125, 250, and 500 μM tungstate (A) or 0, 160, and 320 μM molybdate (B).

patterns observed with tungstate, an analogue of orthophosphate. Previous studies carried out with phosphonatase showed that tungstate is a competitive inhibitor versus phosphonoacetaldehyde with a K_i of 50 μM (*61*). The X-ray crystal structure of phosphonatase shows tungstate bound to the active site Arg160 and Mg^{2+} cofactor, and aligned with the Asp12 nucleophile (*61*). Here we show in Figure 9 that both tungstate and molybdate act as uncompetitive inhibitors of α-G16P-activated β-PGM against the substrate β-G1P. The uncompetitive inhibition observed with tungstate and molybdate is evidence that the substrate and inhibitor compete for different enzyme forms; for instance, the substrate binds to the phosphoenzyme, and the inhibitor binds to the free enzyme. The reciprocal velocity versus inhibitor concentration replots are parabolic, indicating two inhibitor binding sites on the free enzyme and precluding calculation of the inhibition constant.[7] We assume that the two sites correspond to the binding sites for C(6) and C(1) phosphoryl groups of the β-G16P (the "distal" and "transfer" sites, respectively).

Observation of Phospho-β-PGM in the Crystal. In a previous study, the β-PGM from *E. gracilis* was incubated with [^{32}P]-β-G1P and then passed through a Sephadex-25 column (*42*) to show that the enzyme fraction did not contain radiolabel. In the study presented here, we found that the half-life of *L. lactis* phospho-β-PGM in buffer is less than 1 min. Thus emerged the paradox of the aspartyl phosphate group in the structure of β-PGM crystallized in the absence of substrate or activator (*43*). Importantly, HAD phosphotransferases in a mixture with substrate and product, or just product, have been shown to contain a small amount of the phosphoenzyme (*67*−*72*). This suggested that the hydrolysis of the aspartyl phosphate group is reversible. Indeed, alkaline phosphatase is readily phosphorylated via the back reaction with orthophosphate (*79*).

Phosphate had not been deliberately added to the β-PGM crystallization solution containing 16% PEG 3350 and 0.1 M ammonium fluoride (unbuffered, pH 6.5). Therefore, the PEG 3350 lot used to prepare the 16% PEG crystallization solution was tested for phosphate contamination with the Malachite Green phosphate assay (*47*, *48*). The results were positive, and showed that the crystallization solutions had contained 0.45 ± 0.01 mM inorganic phosphate. The ratio of phosphate to total enzyme (0.22 mM) was thus ~2:1, and the ratio of phosphate to enzyme present in the three 1 μg crystals that typically occupy a 2.5 μL well solution was ~13:1. Because the active site of the crystalline enzyme is open to solvent, phosphorylation could have occurred before or after crystallization. In the case of the HAD superfamily member sarcoplasmic reticulum ATPase, added organic solvent substantially increased the level of phosphate-derived phosphoenzyme (*80*) and the high concentrations of PEG used in crystallization might produce a similar effect. The X-ray crystal structure of β-PGM−Mg^{2+} crystals grown from phosphate-free PEG presented herein shows that Asp8 is not phosphorylated.

Summary. This study has demonstrated that Asp8 plays an essential role in β-PGM catalysis, during which it is phosphorylated. The β-PGM aspartyl phosphate group is not stable in water, but the discrimination between solvent and substrate is sufficient to avoid hydrolysis. The efficiency of enzyme phosphorylation and dephosphorylation is determined by the cap domain, which binds with the ligand phosphate group. This interaction stabilizes the cap domain−core domain conformation that, in turn, positions the Asp10 for acid−base catalysis and desolvates the active site. In the cell, β-G1P serves as both a substrate and activator.

REFERENCES

1. Levy, H. R. (1979) Glucose-6-phosphate dehydrogenases, *Adv. Enzymol. Relat. Areas Mol. Biol. 48*, 97−192.
2. Cosgrove, M. S., Gover, S., Naylor, C. E., et al. (2000) An examination of the role of asp-177 in the His-Asp catalytic dyad of *Leuconostoc mesenteroides* glucose 6-phosphate dehydrogenase: X-ray structure and pH dependence of kinetic parameters of the D177N mutant enzyme, *Biochemistry 39*, 15002−15011.
3. Hudson, C. S. (1907) The catalysis by acids and bases of the mutarotation of glucose, *J. Am. Chem. Soc. 29*, 1571−1576.
4. Bailey, J. M., Fishman, P. H., and Pentchev, P. G. (1970) Anomalous mutarotation of glucose 6-phosphate. An example of intramolecular catalysis, *Biochemistry 9*, 1189−1194.
5. Brooks, S. P., Espinola, T., and Suelter, C. H. (1984) Theory and practical application of coupled enzyme reactions: One and two auxiliary enzymes, *Can. J. Biochem. Cell Biol. 62*, 945−955.

[7] The K_{ii} calculated from the reciprocal plot is not the K_i for dissociation of the inhibitor from the enzyme−inhibitor complex but is related to the inhibitor concentration [I] by $K_{ii} = (K_i)^2/(2K_i + [I])$ (*7*).

6. Nakamura, K., Shirokane, Y., and Suzuki, M. (1998) Purification and some properties of β-phosphoglucomutase from *Lactococcus lactis* subsp. cremoris IFO 3427, *J. Ferment. Bioeng. 85*, 350−353.
7. Segel, I. H. (1975) *Enzyme Kinetics: Behavior and Analysis of Rapid Equilibrium and Steady-State Enzyme Systems*, 1st ed., John Wiley & Sons, New York.
8. Ramos, A., Boels, I. C., de Vos, W. M., and Santos, H. (2001) Relationship between glycolysis and exopolysaccharide biosynthesis in *Lactococcus lactis*, *Appl. Environ. Microbiol. 67*, 33−41.
9. Shackelford, G. S., Regni, C. A., and Beamer, L. J. (2004) Evolutionary trace analysis of the α-D-phosphohexomutase superfamily, *Protein Sci. 13*, 2130−2138.
10. Koonin, E. V., and Tatusov, R. L. (1994) Computer analysis of bacterial haloacid dehalogenases defines a large superfamily of hydrolases with diverse specificity. Application of an iterative approach to database search, *J. Mol. Biol. 244*, 125−132.
11. Liu, Y. (1997) Structure of rabbit muscle phosphoglucomutase refined at 2.4 Å resolution, *Acta Crystallogr. D53*, 392−405.
12. Dai, J. B., Liu, Y., Ray, W. J., Jr., and Konno, M. (1992) The crystal structure of muscle phosphoglucomutase refined at 2.7-angstrom resolution, *J. Biol. Chem. 267*, 6322−6337.
13. Regni, C., Tipton, P. A., and Beamer, L. J. (2002) Crystal structure of PMM/PGM: An enzyme in the biosynthetic pathway of *P. aeruginosa* virulence factors, *Structure 10*, 269−279.
14. Regni, C., Naught, L., Tipton, P. A., and Beamer, L. J. (2004) Structural basis of diverse substrate recognition by the enzyme PMM/PGM from P. aeruginosa, *Structure 12*, 55−63.
15. Lahiri, S. D., Zhang, G., Radstrom, P., et al. (2002) Crystallization and preliminary X-ray diffraction studies of β-phosphoglucomutase from *Lactococcus lactus*, *Acta Crystallogr. D58*, 324−326.
16. Manjunath, S., Lee, C. H., VanWinkle, P., and Bailey-Serres, J. (1998) Molecular and biochemical characterization of cytosolic phosphoglucomutase in maize. Expression during development and in response to oxygen deprivation, *Plant Physiol. 117*, 997−1006.
17. Davies, E. J., Tetlow, I. J., Bowsher, C. G., and Emes, M. J. (2003) Molecular and biochemical characterization of cytosolic phosphoglucomutase in wheat endosperm (*Triticum aestivum* L. cv. Axona), *J. Exp. Bot. 54*, 1351−1360.
18. Periappuram, C., Steinhauer, L., Barton, D. L., et al. (2000) The plastidic phosphoglucomutase from *Arabidopsis*. A reversible enzyme reaction with an important role in metabolic control, *Plant Physiol. 122*, 1193−1199.
19. Brautaset, T., Petersen, S., and Valla, S. (1998) An experimental study on carbon flow in *Escherichia coli* as a function of kinetic properties and expression levels of the enzyme phosphoglucomutase, *Biotechnol. Bioeng. 58*, 299−302.
20. Brautaset, T., Petersen, S. B., and Valla, S. (2000) In vitro determined kinetic properties of mutant phosphoglucomutases and their effects on sugar catabolism in *Escherichia coli*, *Metab. Eng. 2*, 104−114.
21. Jolly, L., Ferrari, P., Blanot, D., et al. (1999) Reaction mechanism of phosphoglucosamine mutase from *Escherichia coli*, *Eur. J. Biochem. 262*, 202−210.
22. Jolly, L., Pompeo, F., van Heijenoort, J., et al. (2000) Autophosphorylation of phosphoglucosamine mutase from *Escherichia coli*, *J. Bacteriol. 182*, 1280−1285.
23. Tavares, I. M., Jolly, L., Pompeo, F., et al. (2000) Identification of the *Pseudomonas aeruginosa* glmM gene, encoding phosphoglucosamine mutase, *J. Bacteriol. 182*, 4453−4457.
24. Mio, T., Yamada-Okabe, T., Arisawa, M., and Yamada-Okabe, H. (2000) Functional cloning and mutational analysis of the human cDNA for phosphoacetylglucosamine mutase: Identification of the amino acid residues essential for the catalysis, *Biochim. Biophys. Acta 1492*, 369−376.
25. Ray, W. J., Jr., Burgner, J. W., II, and Post, C. B. (1990) Characterization of vanadate-based transition-state-analogue complexes of phosphoglucomutase by spectral and NMR techniques, *Biochemistry 29*, 2770−2778.
26. Ray, W. J., Jr., and Puvathingal, J. M. (1990) Characterization of a vanadate-based transition-state-analogue complex of phosphoglucomutase by kinetic and equilibrium binding studies. Mechanistic implications, *Biochemistry 29*, 2790−2801.
27. Ray, W. J., Jr., and Post, C. B. (1990) The oxyvanadium constellation in transition-state-analogue complexes of phosphoglucomutase and ribonuclease. Structural deductions from electron-transfer spectra, *Biochemistry 29*, 2779−2789.
28. Ray, W. J., Jr., Post, C. B., Liu, Y., and Rhyu, G. I. (1993) Structural changes at the metal ion binding site during the phosphoglucomutase reaction, *Biochemistry 32*, 48−57.
29. Ray, W. J., Jr., Post, C. B., and Puvathingal, J. M. (1993) Reaction of the isosteric methylenephosphonate analog of α-D-glucose 1-phosphate with phosphoglucomutase. Induced-fit specificity revisited, *Biochemistry 32*, 38−47.
30. Deng, H., Ray, W. J., Jr., Burgner, J. W., II, and Callender, R. (1993) Comparison of vibrational frequencies of critical bonds in ground-state complexes and in a vanadate-based transition-state analog complex of muscle phosphoglucomutase. Mechanistic implications, *Biochemistry 32*, 12984−12992.
31. Rhyu, G. I., Ray, W. J., Jr., and Markley, J. L. (1984) Enzyme-bound intermediates in the conversion of glucose 1-phosphate to glucose 6-phosphate by phosphoglucomutase. Phosphorus NMR studies, *Biochemistry 23*, 252−260.
32. Naught, L. E., and Tipton, P. A. (2001) Kinetic mechanism and pH dependence of the kinetic parameters of *Pseudomonas aeruginosa* phosphomannomutase/phosphoglucomutase, *Arch. Biochem. Biophys. 396*, 111−118.
33. Naught, L. E., Regni, C., Beamer, L. J., and Tipton, P. A. (2003) Roles of active site residues in *Pseudomonas aeruginosa* phosphomannomutase/phosphoglucomutase, *Biochemistry 42*, 9946−9951. Naught, L. E., and Tipton, P. A. (2005) Formation and Reorientation of Glucose 1,6-Bisphosphate in the PMM/PGM Reaction: Transient-State Kinetic Studies, *Biochemistry 44*, 6831−6836.
34. Ye, R. W., Zielinski, N. A., and Chakrabarty, A. M. (1994) Purification and characterization of phosphomannomutase/phosphoglucomutase from *Pseudomonas aeruginosa* involved in biosynthesis of both alginate and lipopolysaccharide, *J. Bacteriol. 176*, 4851−4857.
35. Olvera, C., Goldberg, J. B., Sanchez, R., and Soberon-Chavez, G. (1999) The *Pseudomonas aeruginosa* algC gene product participates in rhamnolipid biosynthesis, *FEMS Microbiol. Lett. 179*, 85−90.
36. Davey, M. E., Caiazza, N. C., and O'Toole, G. A. (2003) Rhamnolipid surfactant production affects biofilm architecture in *Pseudomonas aeruginosa* PAO1, *J. Bacteriol. 185*, 1027−1036.
37. Ray, W. J., Jr., and Long, J. W. (1976) Thermodynamics and mechanism of the PO^{3-} transfer process in the phosphoglucomutase reaction, *Biochemistry 15*, 3993−4006.
38. Ray, W. J., Jr., and Long, J. W. (1976) The thermodynamic and structural differences among the catalytically active complexes of phosphoglucomutase: Metal ion effects, *Biochemistry 15*, 4018−4025.
39. Qian, N., Stanley, G. A., Hahn-Hagerdal, B., and Radstrom, P. (1994) Purification and characterization of two phosphoglucomutases from *Lactococcus lactis* subsp. *lactis* and their regulation in maltose- and glucose-utilizing cells, *J. Bacteriol. 176*, 5304−5311.
40. Mesak, L. R., and Dahl, M. K. (2000) Purification and enzymatic characterization of PgcM: A β-phosphoglucomutase and glucose-1-phosphate phosphodismutase of *Bacillus subtilis*, *Arch. Microbiol. 174*, 256−264.
41. Ben-Zvi, R., and Schramm, M. (1961) A phosphoglucomutase specific for β-glucose-1-phosphate, *J. Biol. Chem. 236*, 2186−2189.
42. Belocopitow, E., and Marechal, L. R. (1974) Metabolism of trehalose in *Euglena gracilis*. Partial purification and some properties of phosphoglucomutase acting on β-glucose 1-phosphate, *Eur. J. Biochem. 46*, 631−637.
43. Lahiri, S. D., Zhang, G., Dunaway-Mariano, D., and Allen, K. N. (2002) Caught in the act: The structure of phosphorylated β-phosphoglucomutase from *Lactococcus lactis*, *Biochemistry 41*, 8351−8359.
44. Lahiri, S. D., Zhang, G., Dunaway-Mariano, D., and Allen, K. N. (2003) The pentacovalent phosphorus intermediate of a phosphoryl transfer reaction, *Science 299*, 2067−2071.
45. Allen, K. N., and Dunaway-Mariano, D. (2004) Phosphoryl group transfer: Evolution of a catalytic scaffold, *Trends Biochem. Sci. 29*, 495−503.
46. Lu, Z., Dunaway-Mariano, D., and Allen, K. N. (2005) HAD superfamily phosphotransferase substrate diversification: Structure and function analysis of the HAD subclass IIB sugar phosphatase BT4131, *Biochemistry* (in press).

47. Harder, K. W., Owen, P., Wong, L. K., et al. (1994) Characterization and kinetic analysis of the intracellular domain of human protein tyrosine phosphatase beta (HPTP beta) using synthetic phosphopeptides, *Biochem. J. 298* (Part 2), 395−401.
48. Martin, B., Pallen, C. J., Wang, J. H., and Graves, D. J. (1985) Use of fluorinated tyrosine phosphates to probe the substrate specificity of the low molecular weight phosphatase activity of calcineurin, *J. Biol. Chem. 260*, 14932−14937.
49. Bradford, M. M. (1976) A rapid and sensitive method for the quantitation of microgram quantities of protein utilizing the principle of protein-dye binding, *Anal. Biochem. 72*, 248−254.
50. Jancarik, J., and Kim, S. H. (1991) Sparse-Matrix Sampling: A screening method for crystallization of proteins, *J. Appl. Crystallogr. 24*, 409−411.
51. Otwinowski, Z., and Minor, W. (1997) Processing of X-ray diffraction data collected in oscillation mode, *Methods Enzymol. 276*, 307−326.
52. Vagin, A., and Teplyakov, A. (2000) An approach to multi-copy search in molecular replacement, *Acta Crystallogr. D56* (Part 12), 1622−1624.
53. Jones, T. A., Zou, J. Y., Cowan, S. W., and Kjeldgaard, M. (1991) Improved methods for building protein models in electron density maps and the location of errors in these models, *Acta Crystallogr. A47* (Part 2), 110−119.
54. Brünger, A. T., Adams, P. D., Clore, G. M., et al. (1998) Crystallography & NMR system: A new software suite for macromolecular structure determination, *Acta Crystallogr. D54* (Part 5), 905−921.
55. Brünger, A. T. (1992) The Free R Value: A novel statistical quantity for assessing the accuracy of crystal structures, *Nature 355*, 472−474.
56. Cleland, W. W. (1979) Statistical analysis of enzyme kinetic data, *Methods Enzymol. 63*, 103−138.
57. Hayward, S., Kitao, A., and Berendsen, H. J. (1997) Model-free methods of analyzing domain motions in proteins from simulation: A comparison of normal mode analysis and molecular dynamics simulation of lysozyme, *Proteins 27*, 425−437.
58. Tremblay, L., Zhang, G., Dai, J., et al. (2005) Chemical confirmation of the oxyphosphorane-β-phosphoglucomutase complex, *J. Am. Chem. Soc. 127*, 5298−5299.
59. Zhang, G., Mazurkie, A. S., Dunaway-Mariano, D., and Allen, K. N. (2002) Kinetic evidence for a substrate-induced fit in phosphonoacetaldehyde hydrolase catalysis, *Biochemistry 41*, 13370−13377.
60. Zhang, G., Morais, M. C., Dai, J., et al. (2004) Investigation of metal ion binding in phosphonoacetaldehyde hydrolase identifies sequence markers for metal-activated enzymes of the HAD enzyme superfamily, *Biochemistry 43*, 4990−4997.
61. Morais, M. C., Zhang, W., Baker, A. S., et al. (2000) The crystal structure of *Bacillus cereus* phosphonoacetaldehyde hydrolase: Insight into catalysis of phosphorus bond cleavage and catalytic diversification within the HAD enzyme superfamily, *Biochemistry 39*, 10385−10396.
62. Liu, J. Q., Kurihara, T., Miyagi, M., et al. (1995) Reaction mechanism of L-2-haloacid dehalogenase of *Pseudomonas* sp. YL. Identification of Asp10 as the active site nucleophile by ^{18}O incorporation experiments, *J. Biol. Chem. 270*, 18309−18312.
63. Lee, S.-L., Hepburn, T. W., Swartz, W. H., et al. (1992) Stereochemical probe for the mechanism of phosphorus−carbon bond cleavage catalyzed by the *Bacillus cereus* phosphonoacetaldehyde hydrolase, *J. Am. Chem. Soc. 114*, 7346−7354.
64. Webb, M. R., and Trentham, D. R. (1981) The stereochemical course of phosphoric residue transfer catalyzed by sarcoplasmic reticulum ATPase, *J. Biol. Chem. 256*, 4884−4887.
65. Cho, H., Wang, W., Kim, R., et al. (2001) BeF_3^- acts as a phosphate analog in proteins phosphorylated on aspartate: Structure of a BeF_3^- complex with phosphoserine phosphatase, *Proc. Natl. Acad. Sci. U.S.A. 98*, 8525−8530.
66. Rinaldo-Matthis, A., Rampazzo, C., Reichard, P., et al. (2002) Crystal structure of a human mitochondrial deoxyribonucleotidase, *Nat. Struct. Biol. 9*, 779−787.
67. Deshpande, R. A., and Wilson, T. E. (2004) Identification of DNA 3′-phosphatase active site residues and their differential role in DNA binding, Mg^{2+} coordination, and catalysis, *Biochemistry 43*, 8579−8589.
68. Pirard, M., Collet, J. F., Matthijs, G., and Van Schaftingen, E. (1997) Comparison of PMM1 with the phosphomannomutases expressed in rat liver and in human cells, *FEBS Lett. 411*, 251−254.
69. Seal, S. N., and Rose, Z. B. (1987) Characterization of a phosphoenzyme intermediate in the reaction of phosphoglycolate phosphatase, *J. Biol. Chem. 262*, 13496−13500.
70. Collet, J. F., Gerin, I., Rider, M. H., et al. (1997) Human L-3-phosphoserine phosphatase: Sequence, expression and evidence for a phosphoenzyme intermediate, *FEBS Lett. 408*, 281−284.
71. Collet, J. F., Stroobant, V., Pirard, M., et al. (1998) A new class of phosphotransferases phosphorylated on an aspartate residue in an amino-terminal DXDX(T/V) motif, *J. Biol. Chem. 273*, 14107−14112.
72. Collet, J. F., Stroobant, V., and Van Schaftingen, E. (2002) Evidence for phosphotransferases phosphorylated on aspartate residue in N-terminal DXDX(T/V) motif, *Methods Enzymol. 354*, 177−188.
73. Zhang, G., Allen, K. N., and Dunaway-Mariano, D. (2003) Enzymatic synthesis of radiolabeled phosphonoacetaldehyde, *Anal. Biochem. 322*, 233−237.
74. Choe, J. Y., Iancu, C. V., Fromm, H. J., and Honzatko, R. B. (2003) Metaphosphate in the active site of fructose-1,6-bisphosphatase, *J. Biol. Chem. 278*, 16015−16020.
75. Qian, N., Stanley, G. A., Bunte, A., and Radstrom, P. (1997) Product formation and phosphoglucomutase activities in *Lactococcus lactis*: Cloning and characterization of a novel phosphoglucomutase gene, *Microbiology 143* (Part 3), 855−865.
76. Levander, F., Andersson, U., and Radstrom, P. (2001) Physiological role of β-phosphoglucomutase in *Lactococcus lactis*, *Appl. Environ. Microbiol. 67*, 4546−4553.
77. Marechal, L. R., and Belocopitow, E. (1974) Metabolism of trehalose in *Euglena gracilis*. β-Glucose 1,6-bisphosphate, activation factor of phosphoglucomutase for β-glucose 1-phosphate, *Eur. J. Biochem. 42*, 45−50.
78. Ray, W. J., Jr., Long, J. W., and Owens, J. D. (1976) An analysis of the substrate-induced rate effect in the phosphoglucomutase system, *Biochemistry 15*, 4006−4017.
79. Gettins, P., and Coleman, J. E. (1983) ^{31}P nuclear magnetic resonance of phosphoenzyme intermediates of alkaline phosphatase, *J. Biol. Chem. 258*, 408−416.
80. Vieyra, A., Mintz, E., Lowe, J., and Guillain, F. (2004) Ca^{2+} binding to sarcoplasmic reticulum ATPase phosphorylated by P_i reveals four thapsigargin-sensitive Ca^{2+} sites in the presence of ADP, *Biochim. Biophys. Acta 1667*, 103−113.

BI050558P